Research Article | Vol. 26, No. 12 | 11 Jun 2018 | OPTICS EXPRESS 15539
Optics EXPRESS

Optical fibre-tip probes for SERS: numerical study for design considerations

TANYA HUTTER,[1,*] STEPHEN R. ELLIOTT,[1] AND SUMEET MAHAJAN[2]

[1]*Department of Chemistry, University of Cambridge, Lensfield Road, Cambridge CB2 1EW, UK*
[2]*Institute for Life Sciences and Department of Chemistry, University of Southampton, Highfield, Southampton SO17 1BJ, UK*
**tf269@cam.ac.uk*

Abstract: Enhancement of sub-wavelength optical fields using sub-micron plasmonic probes has found many applications in chemical, material, biological and medical sciences. The enhancement is via localised surface-plasmon resonance (LSPR) which enables the highly sensitive vibrational-spectroscopy technique of surface-enhanced Raman scattering (SERS). Combining SERS with optical fibres can allow the monitoring of biochemical reactions *in situ* with high resolution. Here, we study the electromagnetic-field enhancement of a tapered optical fibre-tip coated with gold nanoparticles (AuNPs) using finite-element simulations. We investigate the electric-field enhancement associated with metallic NPs and study the effect of parameters such as tip-aperture radius, cone angle, nanoparticle size and gaps between them. Our study provides an understanding of the design and application of metal-nanoparticle-coated optical-fibre-tip probes for SERS. The approach of using fibre-coupled delivery adds flexibility and simplifies the system requirements in SERS, making it suitable for cellular imaging and mapping bio-interfaces.

OCIS codes: (060.2370) Fiber optics sensors; (240.6680) Surface plasmons; (240.6695) Surface-enhanced Raman scattering.

References and links

1. R. Boitor, F. Sinjab, S. Strohbuecker, V. Sottile, and I. Notingher, "Towards quantitative molecular mapping of cells by Raman microscopy: using AFM for decoupling molecular concentration and cell topography," Faraday Discuss. **187**, 199–212 (2016).
2. G. Kostovski, D. J. White, A. Mitchell, M. W. Austin, and P. R. Stoddart, "Nanoimprinted optical fibres: Biotemplated nanostructures for SERS sensing," Biosens. Bioelectron. **24**(5), 1531–1535 (2009).
3. D. J. White, A. P. Mazzolini, and P. R. Stoddart, "Fabrication of a range of SERS substrates on nanostructured multicore optical fibres," J. Raman Spectrosc. **38**(4), 377–382 (2007).
4. K. Gramotnev and S. I. Bozhevolnyi, "Plasmonics beyond the diffraction limit," Nat. Photonics **4**(2), 83–91 (2010).
5. S. Nie and S. R. Emory, "Probing Single Molecules and Single Nanoparticles by Surface-Enhanced Raman Scattering," Science **275**(5303), 1102–1106 (1997).
6. K. Kneipp, Y. Wang, H. Kneipp, L. T. Perelman, I. Itzkan, R. R. Dasari, and M. S. Feld, "Single Molecule Detection Using Surface-Enhanced Raman Scattering (SERS)," Phys. Rev. Lett. **78**(9), 1667–1670 (1997).
7. E. C. Le Ru, M. Meyer, and P. G. Etchegoin, "Proof of Single-Molecule Sensitivity in Surface Enhanced Raman Scattering (SERS) by Means of a Two-Analyte Technique," J. Phys. Chem. B **110**(4), 1944–1948 (2006).
8. J. Taylor, A. Huefner, L. Li, J. Wingfield, and S. Mahajan, "Nanoparticles and intracellular applications of surface-enhanced Raman spectroscopy," Analyst (Lond.) **141**(17), 5037–5055 (2016).
9. J. Kneipp, H. Kneipp, B. Wittig, and K. Kneipp, "Novel optical nanosensors for probing and imaging live cells," Nanomedicine (Lond.) **6**(2), 214–226 (2010).
10. Y. C. Cao, R. Jin, J. M. Nam, C. S. Thaxton, and C. A. Mirkin, "Raman dye-labeled nanoparticle probes for proteins," J. Am. Chem. Soc. **125**(48), 14676–14677 (2003).
11. Y. C. Cao, R. Jin, and C. A. Mirkin, "Nanoparticles with Raman spectroscopic fingerprints for DNA and RNA detection," Science **297**(5586), 1536–1540 (2002).
12. A. Huefner, W. L. Kuan, K. H. Müller, J. N. Skepper, R. A. Barker, and S. Mahajan, "Characterization and Visualization of Vesicles in the Endo-Lysosomal Pathway with Surface-Enhanced Raman Spectroscopy and Chemometrics," ACS Nano **10**(1), 307–316 (2016).

#325486 https://doi.org/10.1364/OE.26.015539
Journal © 2018 Received 8 Mar 2018; revised 23 Apr 2018; accepted 24 Apr 2018; published 6 Jun 2018

Optics EXPRESS

13. D. C. Rodrigues, M. L. de Souza, K. S. Souza, D. P. dos Santos, G. F. S. Andrade, and M. L. A. Temperini, "Critical assessment of enhancement factor measurements in surface-enhanced Raman scattering on different substrates," Phys. Chem. Chem. Phys. **17**(33), 21294–21301 (2015).
14. F. Latorre, S. Kupfer, T. Bocklitz, D. Kinzel, S. Trautmann, S. Gräfe, and V. Deckert, "Spatial resolution of tip-enhanced Raman spectroscopy - DFT assessment of the chemical effect," Nanoscale **8**(19), 10229–10239 (2016).
15. F. I. Baida, D. Van Labeke, and Y. Pagani, "Body-of-revolution FDTD simulations of improved tip performance for scanning near-field optical microscopes," Opt. Commun. **225**(4-6), 241–252 (2003).
16. G. Louarn, S. Taleb, and S. Cuenot, "Prediction of the Transmitted Light Through a Nano-Aperture of SNOM Probes," in *Proceedings of the COMSOL Users Conference Paris* (2006).
17. A. S. Lapchuk, S. K. Yun, V. Yurlov, J. H. Song, S. An, and I. Nevirkovets, "Numerical simulation of characteristics of near-field microstrip probe having pyramidal shape," J. Opt. Soc. Am. A **24**(8), 2407–2417 (2007).
18. A. Drezet, M. J. Nasse, S. Huant, and J. C. Woehl, "The optical near-field of an aperture tip," Europhys. Lett. **66**(1), 41–47 (2004).
19. R. Müller and C. Lienau, "Propagation of femtosecond optical pulses through uncoated and metal-coated near-field fiber probes," Appl. Phys. Lett. **76**(23), 3367–3369 (2000).
20. T. J. Antosiewicz and T. Szoplik, "Description of near- and far-field light emitted from a metal-coated tapered fiber tip," Opt. Express **15**(12), 7845–7852 (2007).
21. M. I. Bakunov, S. B. Bodrov, and M. Hangyo, "Intermode conversion in a near-field optical fiber probe," J. Appl. Phys. **96**(4), 1775–1780 (2004).
22. L. Liu and S. He, "Design of metal-cladded near-field fiber probes with a dispersive body-of-revolution finite-difference time-domain method," Appl. Opt. **44**(17), 3429–3437 (2005).
23. A. Drezet, J. C. Woehl, and S. Huant, "Diffraction by a small aperture in conical geometry: Application to metal-coated tips used in near-field scanning optical microscopy," Phys. Rev. E Stat. Nonlin. Soft Matter Phys. **65**(4 4 Pt 2B), 046611 (2002).
24. Y. Zhang, A. Dhawan, and T. Vo-Dinh, "Design and Fabrication of Fiber-Optic Nanoprobes for Optical Sensing," Nanoscale Res. Lett. **6**(1), 18 (2011).
25. T. J. Antosiewicz, P. Wróbel, and T. Szoplik, "Nanofocusing of radially polarized light with dielectric-metal-dielectric probe," Opt. Express **17**(11), 9191–9196 (2009).
26. A. Bouhelier, J. Renger, M. R. Beversluis, and L. Novotny, "Plasmon-Coupled Tip-enhanced Near-Field Optical Microscopy," J. Microsc. **210**(3), 220–224 (2003).
27. N. A. Janunts, K. S. Baghdasaryan, K. Nerkararyan, and B. Hecht, "Excitation and superfocusing of surface plasmon polaritons on a silver-coated optical fiber tip," Opt. Commun. **253**(1-3), 118–124 (2005).
28. W. Ding, S. R. Andrews, and S. A. Maier, "Internal excitation and superfocusing of surface plasmon polaritons on a silver-coated optical fiber tip," Phys. Rev. A **75**(6), 063822 (2007).
29. K. Kato, A. Ono, W. Inami, and Y. Kawata, "Plasmonic nanofocusing using a metal-coated axicon prism," Opt. Express **18**(13), 13580–13585 (2010).
30. E. A. Vitol, Z. Orynbayeva, M. J. Bouchard, J. Azizkhan-Clifford, G. Friedman, and Y. Gogotsi, "In Situ Intracellular Spectroscopy with Surface Enhanced Raman Spectroscopy (SERS)-Enabled Nanopipettes," ACS Nano **3**(11), 3529–3536 (2009).
31. Y. B. Tan, J. M. Zou, and N. Gu, "Preparation of Stabilizer-Free Silver Nanoparticle-Coated Micropipettes as Surface-Enhanced Raman Scattering Substrate for Single Cell Detection," Nanoscale Res. Lett. **10**(1), 417 (2015).
32. J. P. Scaffidi, M. K. Gregas, V. Seewaldt, and T. Vo-Dinh, "SERS-based plasmonic nanobiosensing in single living cells," Anal. Bioanal. Chem. **393**(4), 1135–1141 (2009).
33. Z. Chen, Z. Dai, N. Chen, S. Liu, F. Pang, B. Lu, and T. Wang, "Gold Nanoparticles-Modified Tapered Fiber Nanoprobe for Remote SERS Detection," IEEE Photonics Technol. Lett. **26**(8), 777–780 (2014).
34. J. Cao and Q. Mao, "Tapered Optical Fiber Probe with a Double–substrate Strategy for Surface–enhanced Raman Scattering Detection," ChemistrySelect **1**(8), 1784–1788 (2016).
35. D. Jin, Y. Bai, H. Chen, S. Liu, N. Chen, J. Huang, S. Huang, and Z. Chen, "SERS detection of expired tetracycline hydrochloride with an optical fiber nano-probe," Anal. Methods **7**(4), 1307–1312 (2015).
36. J. Cao and J. Wang, "Development of Ag nanopolyhedra based fiber-optic probes for high performance SERS detection," New J. Chem. **39**(4), 2421–2424 (2015).
37. W. Xu, Z. Chen, N. Chen, H. Zhang, S. Liu, X. Hu, J. Wen, and T. Wang, "SERS Taper-Fiber Nanoprobe Modified by Gold Nanoparticles Wrapped with Ultrathin Alumina Film by Atomic Layer Deposition," Sensors (Basel) **17**(3), 467 (2017).
38. P. Savaliya and A. Dhawan, "Tapered fiber nanoprobes: plasmonic nanopillars on tapered optical fiber tips for large EM enhancement," Opt. Lett. **41**(19), 4582–4585 (2016).
39. J. D. Driskell, R. J. Lipert, and M. D. Porter, "Labeled Gold Nanoparticles Immobilized at Smooth Metallic Substrates: Systematic Investigation of Surface Plasmon Resonance and Surface-Enhanced Raman Scattering," J. Phys. Chem. B **110**(35), 17444–17451 (2006).
40. C. E. Talley, L. Jusinski, C. W. Hollars, S. M. Lane, and T. Huser, "Intracellular pH Sensors Based on Surface-Enhanced Raman Scattering," Anal. Chem. **76**(23), 7064–7068 (2004).
41. L. Novotny and B. Hecht, *Principles of Nano-Optics* (Cambridge University Press, 2011).

Optics EXPRESS

42. X. Ni, Z. Liu, and A. V. Kildishev, "PhotonicsDB: Optical Constants" (2010), *http://nanohub.org/resources/PhotonicsDB*.
43. T. Hutter, S. R. Elliott, and S. Mahajan, "Interaction of metallic nanoparticles with dielectric substrates: effect of optical constants," Nanotechnology **24**(3), 035201 (2013).

1. Introduction

It is often desirable to measure physiological and biological parameters with a high spatial resolution at a preferred location. Local chemical information (provided by techniques such as Raman spectroscopy) can be extremely important in biology, medicine and forensics [1]. To achieve this, spectroscopic probes can be used [2,3]; however, in order to measure with high spatial resolution, it is desirable to localise the light strongly to dimensions below the optical wavelength. For this purpose, dielectric fibres/waveguides cannot be used, because, as the dimensions decrease, the extent of the evanescent field outside the physical dimensions of the waveguide increases and the light cannot be confined. However, by using metallic waveguides or metal-based structures that support surface plasmons, light can be confined below the diffraction limit [4].

Surface-enhanced Raman scattering (SERS) is a powerful vibrational spectroscopy technique capable of single-molecule detection [5–7]. It is increasingly being used for probing and imaging live cells, to provide molecular structural information on their cellular environment [8]. Measurement of intrinsic cellular molecules in the local optical fields of the metallic nanoparticles can be done in live cells [9]. Metallic nanostructures also can be used with a "reporter molecule" attached to gold and silver nanoparticles instead of using fluorescent tags [10, 11]. By providing the specific SERS spectrum of the reporter, the location of the nanoparticles can be discerned. However, since metal nanoparticles enhance the Raman signatures of molecules in their immediate environment, they can also be used as label-free or reporter-free SERS probes inside cells [12]. In SERS, while the detection is in the far-field, the molecules are interrogated in the near-field of the metallic nanostructures.

On the other hand, in near-field scanning optical microscopy (SNOM), a tapered optical fibre tip is used to scan a sample at a few nanometers from the sample surface. Tip-enhanced Raman spectroscopy (TERS) is another technique wherein a metal-coated (aperture-less) tip (typically a plasmonically active AFM tip) is used. In both cases, the tip is usually coated with a thin metal layer for which in the case of SNOM a small aperture remains uncoated. The aperture normally has a diameter of 30-50 nm to provide high lateral resolution; however, this results in very low light throughput, so there has been much interest in improving such probes. Raman enhancement of signals with both SNOM and TERS are possible but comparing enhancement factors, especially of substrates which are distinct from each other and have different optical properties, is a challenge and can be misleading [13]. Hence solid-coated tips and nanoparticle-coated tips cannot be compared directly as the enhancements they will generate will depend on the respective optical and nanoscale properties. However, the resolution of tips is determined by the aperture or the curvature of the tip, respectively. It follows intuitively that therefore a solid tip can in principle have atomic resolution (sub-nm), as demonstrated by Deckert et al., while a fibre-tip will have a resolution determined by the smallest aperture possible to be constructed, which is likely to be a few nm [14]. A lot of effort has been focused on designing such probes numerically and experimentally to study metal-coated fibre-tips for near-field optical microscopy [15–24], as well as metal-coated aperture-less fibre tips [25–29]. The use of glass capillaries (micropipettes) with sub-micron tips, coated with gold nanoparticles (NPs) for intracellular analysis and for single-cell detection, has been also reported [30, 31].

Low light throughput can be overcome by using optical fibres that can be used to guide the light (laser light and/or SERS signal) to and from a sample, allowing remote measurements at a very localised spot. Vo-Dinh et al. have demonstrated a pH-sensitive plasmonics-active fibre-optic nanoprobe for intracellular bioanalysis in single living human cells using SERS [32]. These authors used an optical tip with a diameter smaller than 100 nm,

Optics EXPRESS

coated with a 6 nm layer of silver and functionalised with para-mercaptobenzoic acid (pMBA) as a pH reporter. Gold nanoparticles coated on the tip surface of a tapered multimode optical fibre have been used for recording SERS spectra by Chen et al; Raman spectra of aqueous solutions of Rhodamine 6G (R6G) with different concentrations were detected in remote-detection mode [33]. Others have also demonstrated the use of highly sensitive metal-nanoparticle-decorated tapered-fibre SERS probes [34–37]. Plasmonic nanostructures at the tips of tapered optical fibres have also been considered [38]. Thus, all this published work has established that tapered fibres can be combined with SERS and this is beneficial for remote monitoring and high resolution *in situ* measurements. Here, we record additional SERS data from exemplar fibres to show that gold-nanoparticle decorated tapered fibres can be used for measurements such as that of pH. However, in this paper, we primarily use the acquisition of SERS from metal-nanoparticle-coated tapered-optical fibres as a motivation for the numerical study.

Although nanoparticle-coated optical-fibre tips for SERS have been experimentally demonstrated, there are no reports on systematic studies or numerical simulations to understand the effect of various geometrical parameters. Here, we present a systematic study for the design of nanoparticle-coated optical-fibre tips for SERS measurements. We consider the simplest case where the laser light is delivered via the fibre and the SERS signal is collected via a microscope objective. We examine the effect of coupling into the nanoparticle gap and the electric-field enhancement in the gap for different geometrical parameters, such as tip radius, cone angle, NP size and gap between the NPs. Three wavelengths, which correspond to the most commonly used Raman-excitation lasers, viz. 532, 633 and 785 nm, are considered.

For SNOM probes, the main challenge is to improve the light transmission through the probe. Here, however, an equally important aspect is to improve the light coupling between the metallic NPs on the fibre-tip surface to obtain the highest enhancements. The design of such probes has to take into account a consideration of the excitation and plasmon coupling in the metal nanoparticles and enhancement factors, which should be optimised for the Raman-excitation wavelength used.

2. Experimental

Optical tapered tips were made by tapering and breaking standard silica fibres using a CO_2 laser-tapering system (P-2000 Sutter Instrument). A graded-index 0.275 NA fibre with a 62.5 μm core and a 125 μm cladding diameter (GIF625, Thorlabs) was used. Surface functionalization of the silica fibre tips was carried out as follows. The fibre-tip was coated with (3-aminopropyl)trimethoxysilane (APTMS). This was done by immersing the tip into 2% APTMS in dry acetone for 1 hour. Then, gold nanoparticles with a diameter of 60 nm were deposited by immersing the tip in an aqueous Au-colloid solution (purchased from BB International) for 2 hours. Following that, the gold NPs on the fibre tip were functionalised with 4-mercaptobenzoic acid (MBA, Mw = 154.19). The solution used had an MBA concentration of 10 mM in absolute ethanol, and the sample was immersed overnight. Buffer solutions of different pH were prepared by mixing appropriate volumes of the following stock solutions: 0.1M potassium hydrogen phosphate (K_2HPO_4, Mw = 204.22), 0.1M potassium dihydrogen phosphate (KH_2PO_4, Mw = 136.09), 0.1M NaOH and 0.1M HCl. The pH of each was confirmed using a pH meter. For the Raman measurements, an InVia Renishaw Raman spectrometer was used. The standard configuration is to deliver and collect the light through a microscope lens in backward-scattering geometry. In order to use it with our fibre-tip probes, a modification had to be used to deliver the light through the optical-fibre probe. External optical components were used to divert the laser beam from inside the spectrometer, focusing the light into a fibre. A micromanipulator (Scientifica LBM-7) was used to hold the fibre probe and move it in three dimensions. The laser light was emitted from the fibre-tip under the microscope lens, which was used to collect the Raman signal and direct it to the detector.

Optics EXPRESS

3. Numerical calculations

Optical simulations were performed using a finite-element method (FEM) with COMSOL Multiphysics, RF Module. A 2D model was employed, which is sufficient to simulate the effect of various parameters on the local field enhancement of the probe. The upper boundary is defined as having a Scattering Boundary condition, at which an excitation field is defined to propagate in the (-y) direction with a polarization either in the x- or z-directions (p- and s-polarizations, respectively). The excitation field amplitude, E_0, was taken to be 1 V/m with a Gaussian beam distribution around x = 0 with a FWHM of two-thirds of the total tip width at the excitation boundary. The field is excited at the upper boundary of the silica fibre and propagates towards the tip. The other boundaries are surrounded by perfectly matched layers (PMLs) with a 200 nm thickness. The tip is rounded on the edges using a radius of half that of the tip. The study was performed for two polarizations, s-polarised light, where the electric field is in the plane of the 2D model, and for p-polarised light, where the field is perpendicular to the plane of the model. A 3D model would normally be a better approach to simulate a real fibre probe; however, in our case, we have an extremely large number of mesh elements due to the nano-particles and nano-sized gaps between them, limiting the possibility of a 3D model. A 2D model, nevertheless, still provides a realistic model, where we study and discuss two polarisations: p-polarisation and s-polarisation. In real fibres, both will result in the same field distribution which will be a combination of the two.

4. Results and discussion

4.1 SERS from nanoparticle-coated fibre tips

Different tip shapes are expected to show different evanescent field distributions, that is, the light leakage will be different. Gradually decreasing the tip diameter will lead to losing light gradually due to concomitant loss of the propagating modes, whereas a probe that has a more abrupt reduction in the diameter will lose most of the light at a single point which acts as a cut-off for many modes.

The difference in the light distributions (for a laser wavelength of 633 nm) between the ends of a flat fibre and a tapered fibre were measured under a microscope and are shown in Fig. 1(a) and 1(b) (the same scale bar is used for the two images). For the flat-fibre end, the light is emitted directly out of the fibre. For a tapered fibre tip, it is seen that the brightest area, with a diameter of about 12 μm, is where most light leaks out from the tip.

In order to observe the sensitivity of SERS signals on tip morphology, we compared a simple flat cleaved fibre end with a tapered fibre tip, both coated with 60 nm gold nanoparticles and functionalised by 4-mercaptobenzoic acid (MBA), a Raman-active molecule. 60 nm gold nanoparticles were selected as they give high SERS-enhancement factors under 633 nm excitation conditions [39] and are optimally suited for coating on the fibre tips from their colloidal suspension.

Figure 1(c) shows SERS spectra of a flat fibre end with a tapered-fibre tip obtained by 633 nm laser excitation. We have also measured the transmission of white light through the tapered tip and the cleaved fibre. For that, a white halogen light source (DH-2000, Ocean Optics) was used by connecting it directly with the fibre. Then, the light from the flat fibre end and tapered tip end was collected using a focusing lens into an additional fibre and to a spectrometer (USB4000, Ocean Optics). While the overall transmission of the tapered fibre was 6 times lower, the SERS intensity is 3 times higher (Fig. 1(c)). This could be due to the focusing effect of the tapered fibre, but also leakage along the taper allowing for better coupling with the gold nanoparticles. This observation thus forms a design consideration for optimisation of the signal-to-noise ratio (SNR) and is therefore studied numerically. Furthermore, we recorded pH-dependent SERS spectra of MBA molecules using an optical fibre tip, coated with Au NPs of 60 nm diameter. Figure 1(c) shows SERS spectra of MBA for pH 4 (blue) and pH 10 (red). The ratios of a pH-responsive peak at 1425 cm^{-1}

Optics EXPRESS

corresponding to the COO- stretching mode, and pH-unresponsive peaks corresponding to the strong ring-breathing mode at 1590 cm^{-1}, were taken. Three different pH solutions were used: pH = 4, 7 and 10. As can be seen in Fig. 1(d), the tapered-fibre tip SERS probe shows a sensitivity to a pH change and the typical pH-dependent behaviour expected with MBA functionalisation [32, 40]. This demonstrates the potential utility of such fibre-based SERS probes and thus serves as a motivation for a systematic optimisation of design considerations.

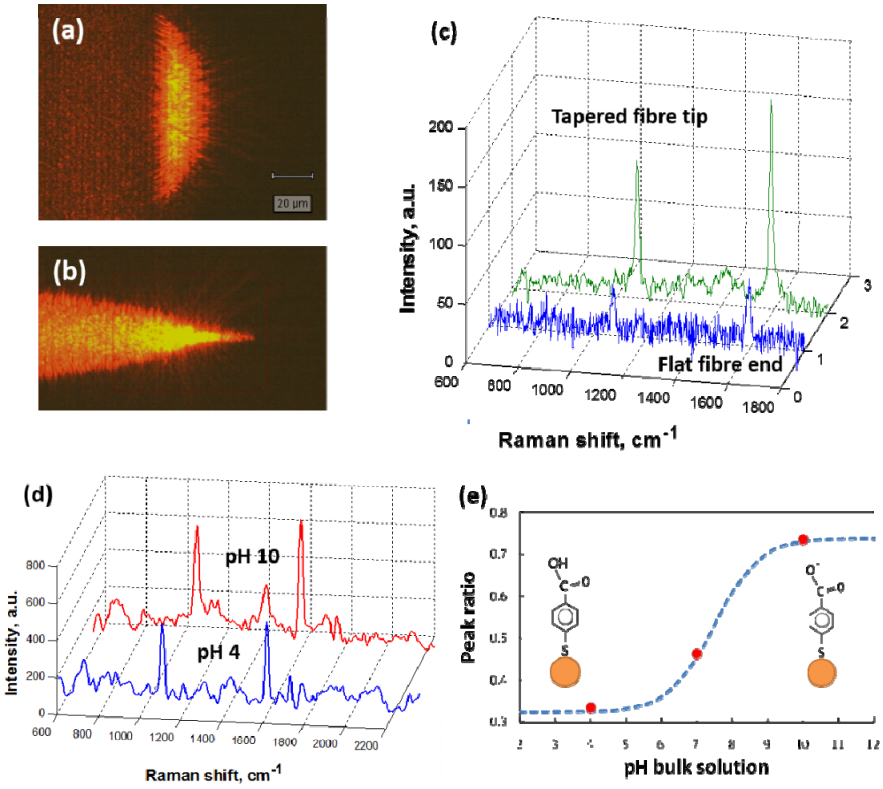

Fig. 1. Measured 633nm laser light distribution in: (a) flat cleaved fibre end; and (b) tapered-fibre tip; (c) SERS spectra of nanoparticles and MBA-coated fibres; (d) SERS spectra of MBA for pH 4 and pH 10; (e) peak ratio (intensity at 1425 cm^{-1} divided by intensity at 1590 cm^{-1}) for different pH buffer solutions.

4.2 Uncoated optical fibre tip

Before investigating other parameters, we first wanted to understand light propagation in an uncoated fibre tip for s- and p-polarisations. A fibre tip with a tip radius of 50 nm, and with a width of 1.6 µm at the excitation boundary and a cone angle of 20.5°, was excited with different wavelengths, and the simulated spatial field distributions at the fibre tip are shown in Fig. 2 for p-polarised light, and in Fig. 3 for s-polarised light, for wavelengths of 500, 700 and 900 nm.

Optics EXPRESS

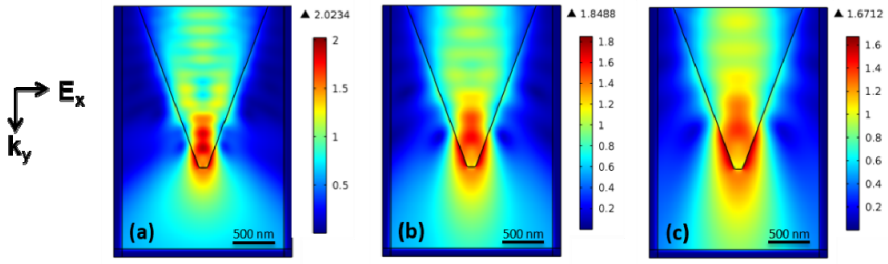

Fig. 2. Simulated spatial distribution of the electric field in a bare silica fibre (50 nm tip radius, 20.5° cone angle) excited by a Gaussian p-polarised light at a wavelength of: (a) 500 nm; (b) 700 nm; and (c) 900 nm.

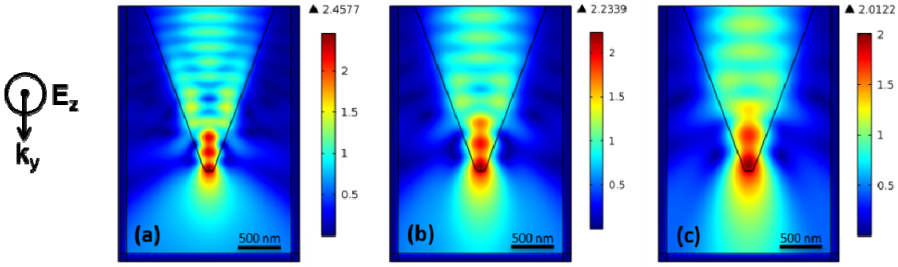

Fig. 3. Simulated spatial distribution of the electric field in a bare silica fibre (50 nm tip radius, 20.5° cone angle) excited by a Gaussian s-polarised light at a wavelength of: (a) 500 nm; (b) 700 nm; and (c) 900 nm.

The tapered conical part of the uncoated silica tip can be represented as a series of discs with decreasing diameters and infinitesimal thicknesses. With each step, the field extends more and more into the surrounding medium, resulting in poor confinement. The extension of the evanescent field, i.e. the fraction of the power propagating in it, depends on the ratio of the wavelength to the radius. The smaller the radius compared to the wavelength, the lesser the field that will propagate in the fibre itself and the more evanescent will be the field. The fraction of the power propagating in the evanescent field also depends on the refractive index of the medium surrounding the fibre. The bigger the refractive index of the surrounding medium, the less confined will be the light in the fibre.

The results show a superposition of incident and reflected light from the silica-air interface, which leads to an intensity maximum at a diameter of approximately half the wavelength, and the best field confinement is roughly for $\lambda/(2n_{silica})$ [41]. Further down the tip, light leaks out to the surrounding air via the evanescent field.

4.3 Fibre tip coated with nanoparticles

Further, a fibre tip that is coated by metallic NPs is considered. The gold NPs are simulated using frequency-dependent real and imaginary parts of the refractive indices taken from [42]. The radius of the NPs is taken as 60 nm and the gap between them is 10 nm. The NPs are placed 1 nm away from the fibre. The spatial electric-field distributions in the fibre tip for p-polarised light are shown in Fig. 4 for wavelengths of 500, 700 and 900 nm. The spatial electric-field distributions in the fibre tip for s-polarised light for wavelengths of 500, 700 and 900 nm are shown in Fig. 5.

Optics EXPRESS

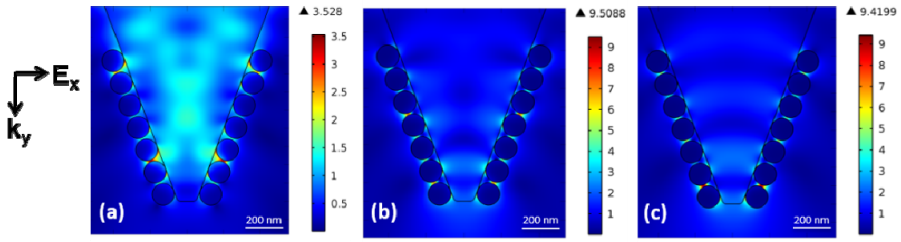

Fig. 4. Spatial distribution of the electric field in a gold nanoparticle-coated silica fibre (50 nm tip radius, 20.5° cone angle) excited by a Gaussian p-polarised light at a wavelength of: (a) 500 nm; (b) 700 nm; and (c) 900 nm.

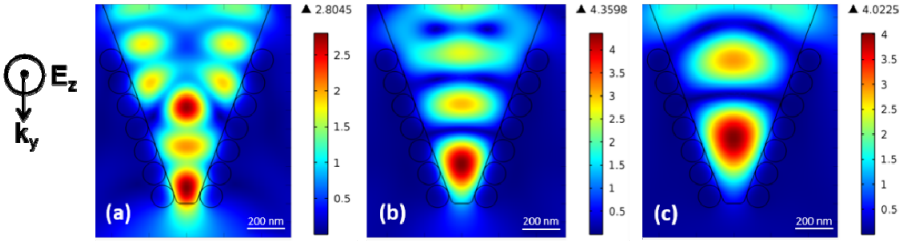

Fig. 5. Spatial distribution of the electric field in a gold nanoparticle-coated silica fibre (50 nm tip radius, 20.5° cone angle) excited by a Gaussian s-polarised light at a wavelength of: (a) 500 nm; (b) 700 nm; and (c) 900 nm.

For p-polarisation, the light leaking out from the fibre is coupled to the surface plasmons between the gold nanoparticles. It can be seen that there is a high electric field between two adjacent NPs at different locations for each wavelength; the 'hot-spot' moves and occurs between different pairs of NPs. High electric-field enhancements of $|E|/|E_0|$ ~9.5 are observed at 700 and 900 nm. For s-polarised light, there is no coupling to the surface plasmons between the gold nanoparticles; however, they do provide a reflective layer, like a mirror, that reflects light back into the tip, creating a standing wave.

To estimate the transmission through the tip for the two polarizations, the electric field 50 nm below the tip is plotted (Fig. 6). For p-polarised light, the lowest transmission of NP-coated fibre tips is at ~570 nm, corresponding to the strong absorption by the Au NPs. A single 60 nm Au NP in air is expected to have absorption at shorter wavelengths; however, because the NPs are near a dielectric fibre and also close to each other, the absorption peak is red-shifted [43]. The low transmission is therefore understandable, as the light is absorbed by the NPs and thus not transmitted. For s-polarization, the highest transmission is at around 550 nm, and then, as the wavelength increases, the transmission decreases. For this polarization, the light is confined by gold NPs, but does not excite plasmon interactions between the NPs (Fig. 5). A decrease in transmission with wavelength is expected, as modes of higher wavelength reach their cut-off at bigger tip diameters.

Optics EXPRESS

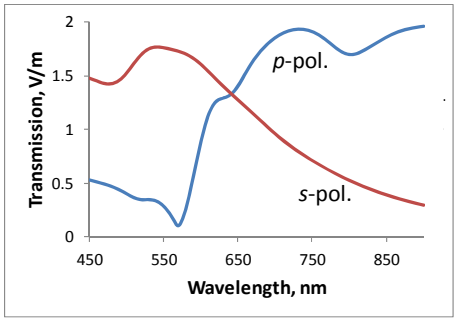

Fig. 6. Transmission at different polarisations as measured 50 nm below a silica fibre tip (50 nm tip radius, 20.5° cone angle) coated with gold nanoparticles of 60 nm diameter, 10 nm gap between the nanoparticles and located 1 nm away from the fibre.

For SERS measurements, enhancement of the electric field is very important. To understand the enhancement in the gaps between the nanoparticles, we have plotted the maximum electric-field values of $|E|/|E_0|$ along a line connecting the NPs in Fig. 7, where E_0 is the excitation field. The oscillations in the spectrum of the p-polarised light actually correspond to the high intensity between different NP pairs (at different locations). For s-polarised light, as expected, no significant enhancement is observed. It is important to note, that for p-polarisation, at the wavelengths of lowest transmission ~570 nm (Fig. 6), the enhancement between the NPs is the highest (Fig. 7), which is due to the light coupling to the surface plasmons between the gold nanoparticles. This result, not surprisingly, shows that for such fibre probes, there is a trade-off between the light throughput and SERS intensity, which should be considered before designing SERS probes for different applications.

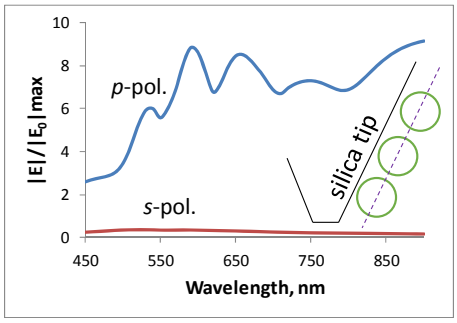

Fig. 7. Plot of maximum electric-field values along a line connecting the nanoparticles. The inset shows the dashed line along the centres of nanoparticles at which the maximum value of the electric field is measured. The silica fibre tip (50 nm tip radius, 20.5° cone angle) coated with gold nanoparticles of 60 nm diameter, 10 nm gap between the nanoparticles and located 1 nm away from the fibre.

In Fig. 8, the electric-field distribution is shown for three different wavelengths in Fig. 8(a)-8(c). The corresponding electric-field values along the line connecting the NPs axis are shown in Fig. 8(c)-8(d). The electric field in the gap between the NPs is much higher compared to that inside the NPs themselves; this results in six peaks, separated by a fixed distance. The highest enhancement is not fixed for one NP pair. At a wavelength of 900 nm, there is a maximum enhancement between the NPs at the tip end.

Optics EXPRESS

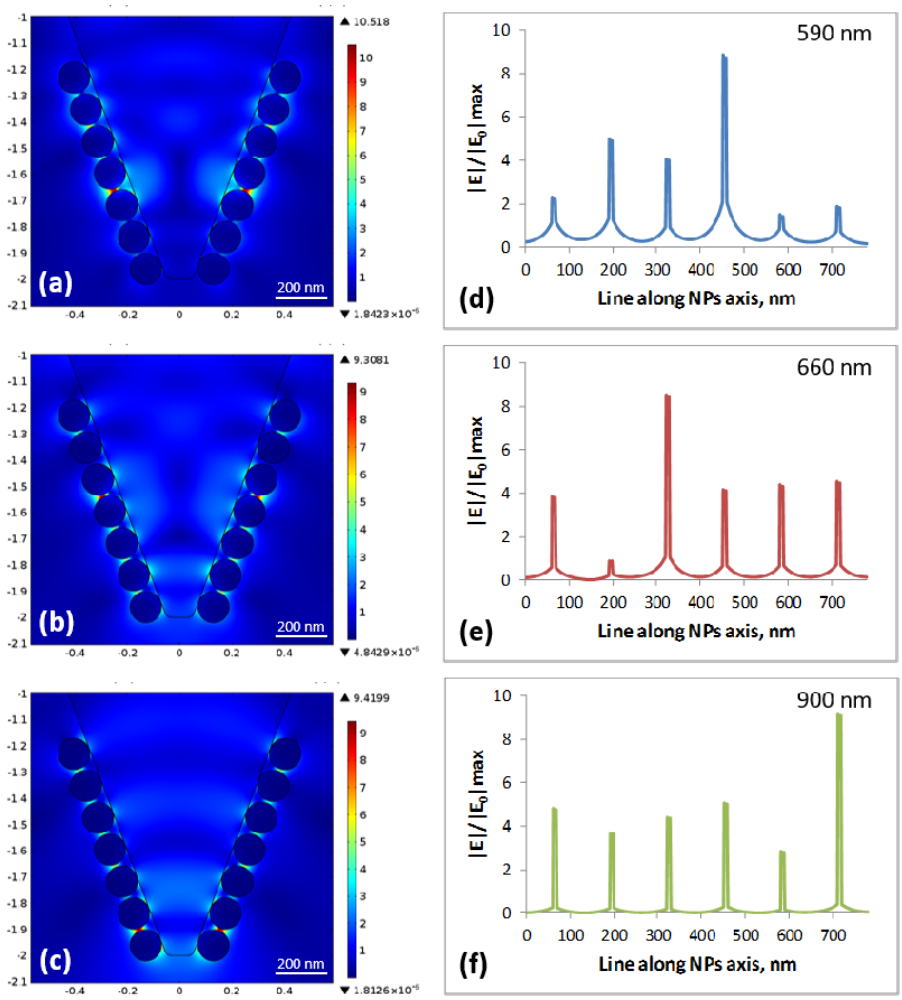

Fig. 8. Electric-field distribution in the gold nanoparticle-coated fibre tip at wavelengths of: (a) 590 nm; (b) 660 nm; and (c) 900 nm. The corresponding electric-field values along a line connecting the NPs' axis at wavelengths of: (d) 590 nm; (e) 660 nm; and (f) 900 nm. The silica fibre tip (50 nm tip radius, 20.5° cone angle) coated with gold nanoparticles of 60 nm diameter, 10 nm gap between the nanoparticles and located 1 nm away from the fibre.

It will now be shown how different geometrical parameters, such as tip radius, cone angle, NP size and gap between the NPs, affect the coupling into the gap and the electric-field enhancement in the gap. Three wavelengths, which correspond to the most commonly used Raman lasers, viz. 532, 633 and 785 nm, are considered.

Effect of fibre-tip aperture size and cone angle

The effect of the radius of the tip on the near-field enhancement between the NPs is shown in Fig. 9(a) for the three laser wavelengths. This is taken as the maximum value along a line connecting the NPs, as shown in the inset of Fig. 7. As before, the radius of the NPs is taken as 60 nm and the gap is 10 nm, and the NPs are 1 nm away from the fibre surface. The aperture radius of the tip was varied from 50 to 500 nm, with a step size of 10 nm. Oscillations in the electric field as the radius of the tip varies are observed for all wavelengths. These oscillations are likely due to the fact that the location of the highest intensity in the gap between each NP pair is not fixed and depends on the tip radius, as the maximum value along the line of all the NPs is measured. The main thing to note is that the

Optics EXPRESS

overall near-field enhancement between the NPs does not change significantly with the tip radius. The bigger the tip, the more modes can propagate in it, and eventually, as they are cut-off, the evanescent field outside the walls of the taper increases to couple with the NPs. This fact relaxes the fabrication condition with respect to the radius of the tip, as it is very difficult to control the exact radius of a tip in practice. It also seems that the enhancement is lowest for 532 nm. This is expected for such a size of closely adjacent NPs which results in plasmon resonances at higher wavelengths.

For a fixed tip radius of 250 nm, the cone angle was varied from 14 to 56°. A plot of the maximum field values along a line connecting the NPs as a function of the cone angle, for laser wavelengths of 532, 633 and 785 nm, is shown in Fig. 9(b). The highest enhancement appears to be at a wavelength of 785 nm for an angle of 35°. Furthermore, at 532 and 633 nm wavelengths, higher cone angles are more effective than lower angles.

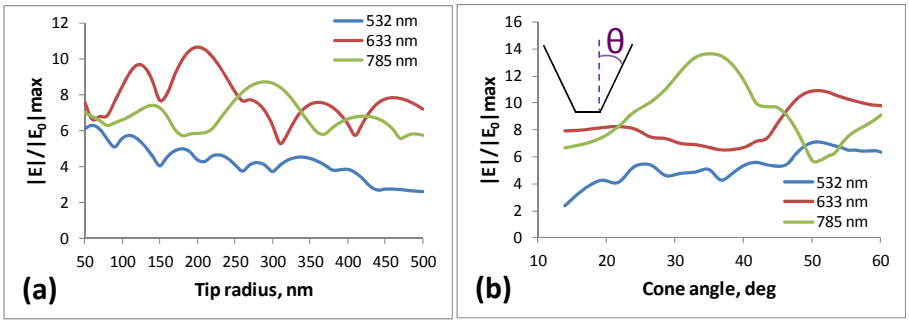

Fig. 9. (a) Plot of maximum electric-field values along a line connecting the nanoparticles as a function of: (a) the radius of the tip for a fixed cone angle of 20.5°; and (b) the cone angle for laser wavelengths of 532, 633 and 785 nm (radius of tip is 250 nm). The inset shows how the cone angle is defined. The silica fibre tip coated with gold nanoparticles of 60 nm diameter, 10 nm gap between the nanoparticles and located 1 nm away from the fibre.

Effect of gap between NPs and their size

The effects of the NP size and gap are shown in Fig. 10(a) and 10(b) for a fixed tip radius of 250 nm and a cone angle of 30°. As expected, as the gap between the NPs increases, the electric field decreases significantly. With respect to the size of the NPs, there is an optimal size for each wavelength: the bigger the wavelength, the bigger the optimal NP size. For 532 nm, it is ~20 nm radius, for 633 nm, it is ~40 nm and for 785 nm, it is ~75 nm.

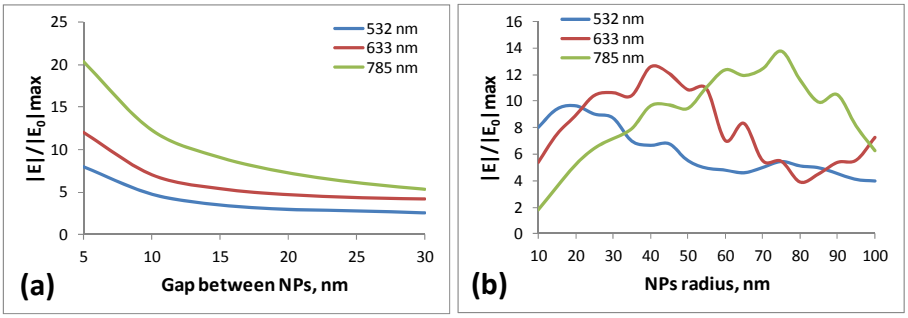

Fig. 10. (a) Plot of maximum electric-field values along a line connecting the nanoparticles as a function of: (a) the gap distance between the 60 nm diameter nanoparticles; and (b) the radius of the nanoparticles with 10 nm gap, for laser wavelengths of 532, 633 and 785 nm for a fixed fibre tip radius of 250 nm and a cone angle of 30°.

Optics EXPRESS

5. Conclusions

Optical simulations provide useful information for the design and performance of nanoparticle-coated tapered optical-fibre SERS probes. In this arrangement, the laser light is delivered to the metallic nanoparticles through the optical fibre via evanescent excitation at the tapered tip. Several geometrical parameters, such as tip radius, cone angle, NPs size and gap between the NPs, were studied for three common Raman laser excitation wavelengths. Creating low-cost and reproducible nano-structured surfaces is a continuing challenge for the SERS community, and usually expensive equipment is required. Our results show that certain parameters, such as tip aperture radius, do not have a significant effect on the electric-field enhancement in the gaps between the nanoparticles. This fact relaxes the fabrication condition with respect to the radius of the tip, which is quite difficult to control. However, the size of the nanoparticles does have an effect on the electric-field enhancement, and for best enhancement, the size should be chosen based on the desired Raman excitation laser. Such nanostructured probes will be able to measure localised Raman signals at desired locations with high sensitivity.

Funding

UK Engineering and Physical Sciences Research Council (EPSRC), United Kingdom for financial support (grants EP/H028757/1, EP/H028757/2), to Trinity College, Cambridge for a PhD studentship and to Darwin College, Cambridge for a Henslow Research Fellowship.